Computational and Structural Biotechnology Journal 23 (2024) 1387–1396

Contents lists available at ScienceDirect

Computational and Structural Biotechnology Journal

journal homepage: www.elsevier.com/locate/csbj

Research Article

Cysteine hyperoxidation rewires communication pathways in the nucleosome and destabilizes the dyad

Yasaman Karami [a], Emmanuelle Bignon [b,*]

[a] Université de Lorraine, CNRS, Inria, LORIA, F-54000 Nancy, France
[b] Université de Lorraine, CNRS, LPCT UMR7019, F-54000 Nancy, France

ARTICLE INFO

Keywords:
DNA compaction
Molecular modeling
Protein structural networks
Post-translational modifications
Epigenetics

ABSTRACT

Gene activity is tightly controlled by reversible chemical modifications called epigenetic marks, which are of various types and modulate gene accessibility without affecting the DNA sequence. Despite an increasing body of evidence demonstrating the role of oxidative-type modifications of histones in gene expression regulation, there remains a complete absence of structural data at the atomistic level to understand the molecular mechanisms behind their regulatory action. Owing to μs time-scale MD simulations and protein communication networks analysis, we describe the impact of histone H3 hyperoxidation (i.e., S-sulfonylation) on the nucleosome core particle dynamics. Our results reveal the atomic-scale details of the intrinsic structural networks within the canonical histone core and their perturbation by hyperoxidation of the histone H3 C110. We show that this modification involves local rearrangements of the communication networks and destabilizes the dyad, and that one modification is enough to induce a maximal structural signature. Our results suggest that cysteine hyperoxidation in the nucleosome core particle might favor its disassembly.

1. Introduction

The regulatory effect of histone proteins post-translational modifications (PTM) onto DNA compaction and gene expression is a timely matter of research. If these modifications offer promising perspectives for the development of epigenetic therapies against a large panel of diseases, we are still far from understanding correctly their independent role on DNA compaction and their combinatorial effect. PTM consist in mostly reversible chemical modifications of amino acids that allow the regulation of proteins' activity after their biosynthesis. There exists a broad spectrum of such modifications, and some of them (phosphorylation, glycosylation, methylation, acetylation) have been the privileged subject of investigations due to the robustness of their detection methods. At the molecular level, histone proteins (H3, H4, H2A, and H2B) assemble to form an octameric core around which ~146 base pairs of DNA are wrapped, resulting in the first level of DNA compaction, the so-called the nucleosome core particle (NCP) – see Fig. 1. Histone proteins share a common fold featuring three main α helices flanked by a C-term and/or N-term additional αhelix (αC and/or αN). Nucleosome aggregation forms the chromatin, which undergoes dynamic structural exchanges between an open state (euchromatin) favoring DNA exposure for gene expression and a compacted state (heterochromatin) associated with gene silencing. Within this complex assembly, DNA compaction is regulated by a plethora of PTM, yet many aspects of the molecular mechanisms underlying this finely-tuned regulation remain to be unraveled.

In this sense, structural biology and computational approaches are of major importance to get insights into the atomistic details underlying these phenomena. The first experimental structure of a NCP was published in 1997 by Luger et al. [2]. Since then, technical improvements (e.g., the advent of cryoelectronic microscopy) led to the deposition of hundreds of NCP structures on the Protein Data Bank (PDB), gathering from mono- to 6-mer NCP assemblies [3] and large NCP-protein complexes. This accumulation of data also allowed to start unraveling the finely-tuned epigenetic regulation of chromatin dynamics by histone PTM and variants exchange, resorting to both experimental and theoretical approaches [4,5]. Yet, structures of NCP harboring PTM marks are rare, and a lot of aspects remain to be uncovered in order to get a better understanding of epigenetic regulation at the molecular level.

It is only recently that oxidative PTM (oxPTM) have gained interest from the biochemical community due to their importance in disease onset and for the development of redox-based therapies. Cysteines are preferential targets for oxidative modifications and act as redox switches in many proteins [6]. They can react with nitric ox-

* Corresponding author.
E-mail address: emmanuelle.bignon@univ-lorraine.fr (E. Bignon).

https://doi.org/10.1016/j.csbj.2024.03.025
Received 13 November 2023; Received in revised form 27 March 2024; Accepted 27 March 2024
Available online 3 April 2024

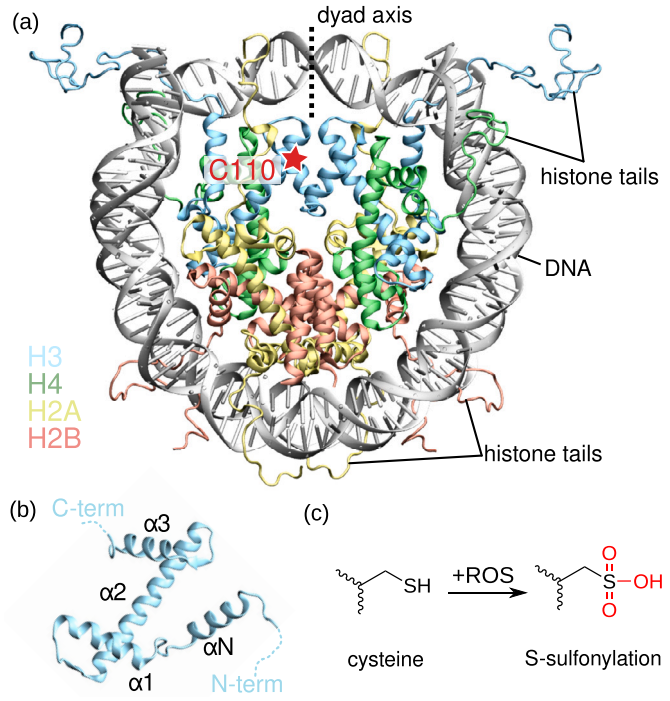

Fig. 1. (a) Structure of a NCP modeled from the 1KX5 PDB [1] with symmetric histone H3 tails. Histone proteins are colored according to their type: H3 in blue, H4 in green, H2A in yellow, and H2B in orange. The position of the C110 residue on one histone H3 copy, that is targeted by oxidative PTM, is marked by a red star. **(b)** Canonical fold of the histone H3, featuring the conserved three main α helices and an additional αN helix in its N-terminal region. Other histone types can exhibit an additional αC as well, e.g., H2B. **(c)** Hyperoxidation of cysteines can induce its S-sulfonylation, which is an irreversible, deleterious oxidative PTM.

ide (S-nitrosylation), glutathione (S-glutathionylation), hydrogen sulfide (S-persulfidation), and can undergo several other types of oxidation. Among the large spectrum of oxidatively-regulated proteins, nuclear proteins such as histones and proteins involved in DNA transcription, replication, and DNA damage repair have recently started to gather attention. Indeed, the activity of several partner proteins of the nucleosome can be regulated by oxPTM, such as histone de-acetylases (class 1 HDAC, sirtuin proteins…) [7,8], transcription factors (STAT3, NF-κB, AP-1…) [9,10], or DNA repair enzymes (O6-alkylguanine-DNA-alkyltransferase, 8-oxoguanine glycosylase…) [11,12], underlying the complexity and richness of oxidative stress and epigenetic processes crosstalk. The oxidation of histone proteins plays an important role in chromatin dynamics modulation, and oxidative stress-related alteration of gene expression is involved in aging and pathogenesis (e.g., cancer, neurodegenerative diseases, respiratory syndrome) [7]. S-glutathionylation of the nucleosome has been shown to promote chromatin opening [13], while S-sulfonylation of histone H3 has been observed under oxidative stress [8]. Yet, the importance of oxidative epiregulation of nucleosomal assemblies has been, until recently, widely neglected and their function and underlying molecular mechanisms remain to be uncovered.

Studies of histone core PTM location suggested that the ones located at the dyad (e.g., H4S47ph, H3K115ac, H3T118ph, H3K122ac) would favor the nucleosome disassembly, while those near the DNA entry/exit (e.g.,H3Y41ph, H3K56ac, H3S57ph) would promote DNA unwrapping without destabilizing the overall structure [14–18]. Besides, computational investigations of the structural effect of H2A variants suggested allosteric effects and communication pathways involving the DNA double-helix [19]. Importantly, the histone H3 cysteine (C110) is located near the dyad but is not in direct contact with the DNA helix, suggesting that its oxidative modification might impact the NCP dynamics in novel ways involving medium- to long-range effects that remain to be described.

Owing to molecular dynamics (MD) simulations and extensive structural post-analysis, we report here the first in-depth description of the NCP intrinsic protein structural networks, and its perturbation by histone H3 S-sulfonylation resulting from cysteine hyperoxidation. We show that this oxidative modification perturbs the DNA dynamics close in the dyad region. Interestingly, our results suggest that the structural perturbation signature of S-sulfonylation is maximal already with a single modified site, with only little additional deformation observed with a second modification. Such perturbation is induced by a rewiring of the local structural network, which results in the perturbation of the H3-H3 interface. We also scrutinized the DNA length and sequence effects onto the NCP protein structural network by considering both α-satellite and 601 Widom DNA sequences, and probed the effect of salt concentration on our results with the S-sulfonylated NCP. Our results provide important insights into the communication pathways within the histone core and their perturbation by an oxidative PTM, which sets the grounds for larger-scale mapping of molecular mechanisms underlying PTM regulation of the NCP dynamics at the atomic scale.

2. Methods

All simulations were performed using the NAMD3 software [20]. System setup and analysis were performed using the AMBERTools20 suite of programs [21] and COMMA2 and Curves+ approaches [22,23]. The VMD 1.9.3 [24] and Pymol 2.5.5 [25] softwares were used for visualization and pictures rendering.

2.1. System preparation

The α-satellite NCP starting structure for MD simulations was taken from Davey et al. crystal structure of the NCP featuring an α-satellite DNA sequence and histone tails (PDB ID 1KX5 [1]). Crystallographic waters and ions were removed. Force field parameters were taken from ff14SB [26], and bsc1 [27] and CUFIX [28] corrections were applied to improve DNA and the disordered tails description.

The sulfonylated NCP starting system was created from the canonical NCP by mutating *in silico* the cysteine 110 of the first copy of histone H3. The modified residue name was set to OCS, consistently to what is found in the literature. Considering the very low pKa (~2) of sulfonated cysteines [29], the deprotonated form of OCS was used, with a total charge of -1. Parameters were generated for the sulfonylated cysteine using the antechamber protocol: i) the structure of the modified cysteine N- and C-term ends were capped by an acetyl (-OCH_3) and a methylamino (-$NHCH_3$) group, respectively; ii) this structure was optimized at the B3LYP/6-311+G** level and a frequency calculation was carried out to ensure that the energy reached a minimum; iii) Mertz-Kollman charges were computed at the HF/6-31+G* level on the optimized structure; iv) the antechamber protocol was used to assign atom types and fit RESP charges; v) charges of the capping atoms were set to 0 and equally distributed on the other atoms to ensure a total charge of -1; vi) the AMBER library file was generated with the removal of capping atoms and the connectivity set onto the N and C atoms of the residue named OCS, using the tleap module of AMBER.

Each system (control = 1KX5 and sulfonylated = 1KX5+OCS) was soaked into a TIP3P truncated octahedral water box applying a 20 Å buffer between the NCP and the edges of the box. A 0.150 M salt concentration was ensured by randomly adding 378 Na^+ and 233 Cl^- ions. In order to evaluate the impact of a second S-sulfonylation (on H3'C110) on the NCP dynamics, a system with two S-sulfonylated sites was simulated. Besides, the salt concentration effect was probed by also simulating a system with one S-sulfonylation site but no NaCl by adding only 145 Na+ counter-ions to neutralize the total charge. The final systems gathered a total of ~400,000 atoms including ~123,000 water molecules.

The OCS parameters and MD input files are available on Github: https://github.com/emmanuellebignon/NCP-OCS-pathways.

2.2. Molecular dynamics simulations

Each system was first subjected to a 30,000-step energy minimization using the conjugate gradient algorithm. Then, four subsequent equilibration runs of 10 ns were carried out at 300 K with decreasing constraints on the biomolecule's atoms. The time step was then increased from 2 fs to 4 fs by using the Hydrogen Mass Repartitioning algorithm [30] in addition to the SHAKE and RATTLE ones [31], and a 2 μs production run was performed in the NPT ensemble. The temperature and the pressure (1 atm) were kept constant using the Langevin thermostat with a 1 ps^{-1} collision frequency and a Langevin piston barostat with a damping time scale of 50 fs and an oscillation period of 100 fs. Electrostatics were treated using the Particle Mesh Ewald approach [32] with a 9 Å cutoff.

For each system (1KX5, 1KX5+OCS, 1KX5+2OCS, 1KX5+OCS no NaCl), six replicates were carried out with random initial velocities in order to ensure the statistical significance of the results, resulting in a total of 48 μs of simulation time. Velocities, box information and coordinates were recorded every 25,000 steps (i.e., every 0.5 ns and 1 ns for the equilibration and production runs, respectively).

MD ensembles of the 601 Widom NCP were taken from a previous study from us and collaborators [33], which consisted in three replicates amounting for a total of ~15 μs performed in the same conditions as the present study.

2.3. Structural analysis

2.3.1. Protein network analysis

For each system, the network of pathways and communication blocks were identified using COMMA2 [22]. In COMMA2, communication pathways are chains of residues that are not adjacent along the sequence, are linked by non-covalent interactions (hydrogen bonds or hydrophobic contacts) and communicate efficiently. Communication efficiency or propensity is expressed as [34]:

$$CP(i,j) = < (d_{ij} - \overline{d_{ij}})^2 > \quad (1)$$

where d_{ij} is the distance between the Cα atoms of residues i and j and d_{ij} is the mean value computed over the entire set of conformations. These pathways form the protein communication network (PCN), in which nodes correspond to the residues of the protein and edges connect residues adjacent in a pathway. COMMA2 extracts connected components from the graph by using depth-first search algorithm to identify the protein dynamical units. These units are referred to as "communication blocks" (see [34] for detailed descriptions).

Hydrogen bonds networks were calculated using the HBPLUS algorithm [35]. This algorithm detects hydrogen bonds between the donor (D) and acceptor (A) atoms using the following geometric criteria: *(i)* maximum distances of 3.9 Å for D-A and 2.5 Å for H-A, *(ii)* minimum value of 90% for D-H-A, H-AAA and D-A-AA angles, where AA is the acceptor antecedent. For every pair of residues, we assigned an interaction strengths as the percentage of conformations in which a hydrogen bond is formed between any atoms of the same pair of residues. We then merged the results from all replicates of each system. We reported hydrogen bonds that are present for more than 40% of the simulation time (with strength values greater than or equal to 0.4). Only the proteins were taken into account for the COMMA2 analysis).

2.3.2. Per residue flexibility contribution

Per residue contribution to the overall flexibility of the system was calculated for DNA and histones, using a PCA-based machine learning script that was successfully used on similar DNA-protein and nucleosomal systems in previous studies [36–38]. In this script, the internal coordinates of the residues are extracted from the MD ensembles, the inverse distance between geometric centers of each residue pair is computed, and a covariance matrix is generated, which eigenmodes and eigenvectors respectively represent the system's modes of motion and their amplitude. The main fluctuations of the system are encrypted in the highest amplitude eigenmodes, and per residue normalized contribution to these modes of motion are calculated that translates their contribution to the overall flexibility of the system.

This analysis has been conducted onto the control and S-sulfonylated systems, taking into account the six MD simulations replicates performed for each system. Calculations for the DNA helix and the protein were performed separately, and the histone tails were not included to prevent statistical noise.

2.3.3. Other structural descriptors

The cpptraj AMBER module was used to calculate all distances and RMSD values, and to perform clustering analysis. For the monitoring of hydrogen bonds/salt bridges distances involving lysines, arginines, aspartates or glutamates side chains, the NZ, CZ (or NH2/NH1 if relevant), CG, and CD atoms were respectively taken into account for the distance calculation. This allowed to avoid monitoring any jumps that could arise from the rotation of the terminal charged moiety. The Curves+ software [23] was used to monitor the DNA structural parameters around the dyad section (between superhelical locations SHL-1 and SHL+1). The structure of the 21-bp section around SHL0 was extracted from the MD ensemble with 1 frame per ns. These structures were submitted to Curves+ analysis and the corresponding statistical values were computed from the results.

Error bars are display as Standard Error of the Means.

3. Results

For sake of clarity, the two sides of the NCP are referred to as face A and face B, and the amino acids of the second copy of each histone are named with an extra apostrophe (e.g., H3'T118).

3.1. Communication blocks and pathways in the native nucleosome core particle

3.1.1. Communication blocks

The protein structural network analysis of the α-satellite NCP reveals fifteen communication blocks within the histone core, i.e. fifteen independent groups of residues that mediate short- and long-range communication pathways within the overall structure - see Fig. 2-a. The arrangement of these blocks on the histone core is mostly symmetric, with seven blocks for each face (A and B) of the NCP.

These communication blocks are distributed along the H2A-H2B and H3-H4 dimers but do not spread to wider architectures. Interestingly, the H2A-H2B dimers are divided in five blocks whereas the H3-H4 dimers exhibit a more compact structure with two main blocks. This could be linked to the fact that the nucleosome is built by the docking of two separate H2A-H2B dimers onto a $(H3\text{-}H4)_2$ tetramer [39].

In each H2A-H2B dimer, the two main blocks involve residues of both H2A and H2B which might be important for the dimer formation. On the first face of the NCP (face A), the biggest block (block 5) involves H2B αC helix and H2A α2 helix. The second biggest (block 3) gathers H2B α2 helix and H2A α3 helix. The three other blocks are located on H2B α1 (block 2) and α3 (block 1), and H2A α3 (block 4). Noteworthy, a slight asymmetry is observed on the other face of the NCP (face B), in which a larger block (block 13) spreads onto H2B αC and H2A α2/α3, with the block gathering H2B α2 helix and H2A α3 helix (block 3 on face A) split in two (blocks 11 and 12).

The H3-H4 dimers exhibit more cohesive blocks. On both faces of the NCP, a large block involves the three H4 main helices and H3 αN/α2/α3 (Block 8/15 on face A/B, respectively), and H3 α1 forms an isolated block (block 7/14). On face A a small block is found in H3' α3 helix, intertwined with the major one, that involves only four amino acids

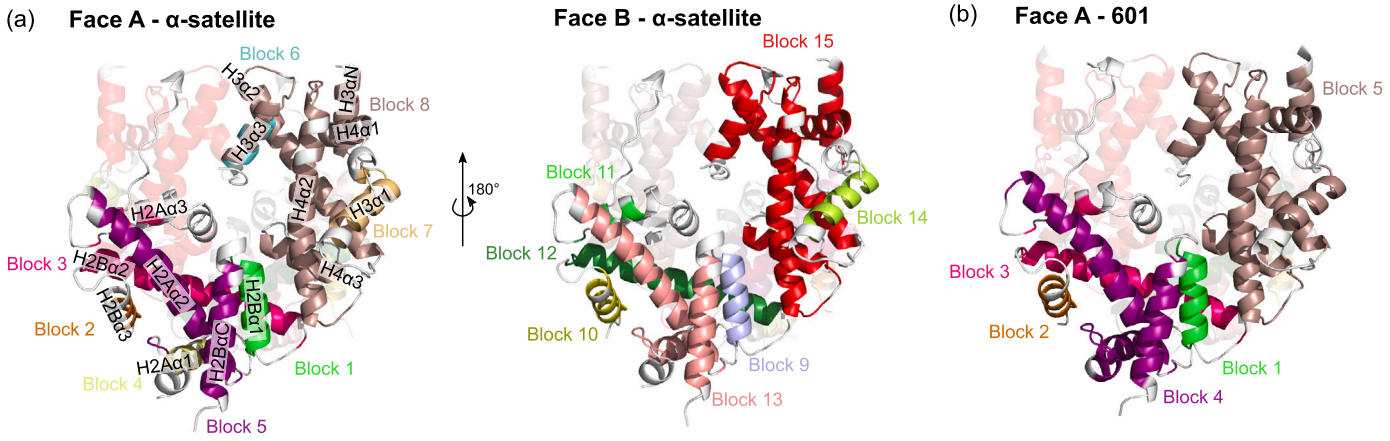

Fig. 2. (a) Communication blocks within the canonical NCP featuring the α-satellite DNA sequence. Due to the intrinsic symmetry of the histone core, the blocks on face A (left) and B (right) of the NCP are mostly equivalent. Histone helices are labeled on Face A. **(b)** Communication blocks with the 601 Widom DNA sequence. Only face A is shown, see Figure S1 for face B. Histone tails are not displayed.

(I111', L113', R115', and I117'). A detailed list of the number of residues in each block is given in Table S1.

Taking advantage of 3x5 μs MD ensembles of the 601 Widom sequence NCP from a previous work [33], we performed the same analysis to get insights into DNA sequence effects onto the histone core communication blocks and pathways. The 601 structure exhibits less (9 instead of 15) but larger communication blocks - see Fig. 2-b. This suggests the existence of longer range communication pathways in the 601 Widom system compared to the α-satellite one. H2A α3 here forms a large block with H2B αC and H2A α2 (block 4, instead of two separated blocks with the α-satellite sequence), and the H3-H4 is involved in a compact isolated block (block 5). The same trend is observed on face B of the 601 NCP, yet it shows even larger communicating regions by the fusion of blocks 1 and 3 - see Figure S1. This tighter communication network could come from the stronger packing of the DNA around the histones, that could sterically reinforce the intrinsic interactions within the histone core by limiting its dynamical behavior.

3.1.2. *Communication pathways*

In order to have a better understanding of the wiring of the communication blocks, communication pathways within the α-satellite NCP structure were scrutinized. The analysis of the communication pathways shed light on a large communication network in which communication hubs could be pinpointed, i.e. the amino acids that might be crucial for the system's structural stability and allosteric regulation - see Fig. 3-a. Very interestingly, the major hubs in the NCP structure are found on histone H3 α2 helix - the full list of hubs in each pathway is given in SI. In both histone H3 copies, the M90-T107 section exhibits the larger hubs in the entire structure. As this helix is involved in the large H3-H4 communication block, it acts as a pivot for long range interactions within this dimer. At the one end, it mediates many pathways involving H4 α1 helices (itself highly connected to H3 αN and H4 α2) - see Fig. 3-b. Of note, the C110 is located next to T107, that appears to be a dense hub, suggesting that the modification of this cysteine might have a crucial impact on the communication pathways that depend on the H3 α2 helix. Indeed, it has been suggested that residues adjacent to communication hubs can as well impact the structure and function of proteins [40]. At the other end of H3 α2 helix, hubs are involved in few connections with other residues of H4 α1, and with the L1 loop right after H3 α1 - see Fig. 3-c. As it is involved in several communication pathways, H4 α1 also harbors quite populated hubs, from K31 to V43.

As already seen in the description of the communication blocks, pathways in the H2A-H2B dimers are much more fragmented than in H3-H4 - see Figure S2-a. Hubs can be pinpointed in H2A α2 (residues L51 to L63) and to a lesser extent in H2B αC (residues A107 to Y118),

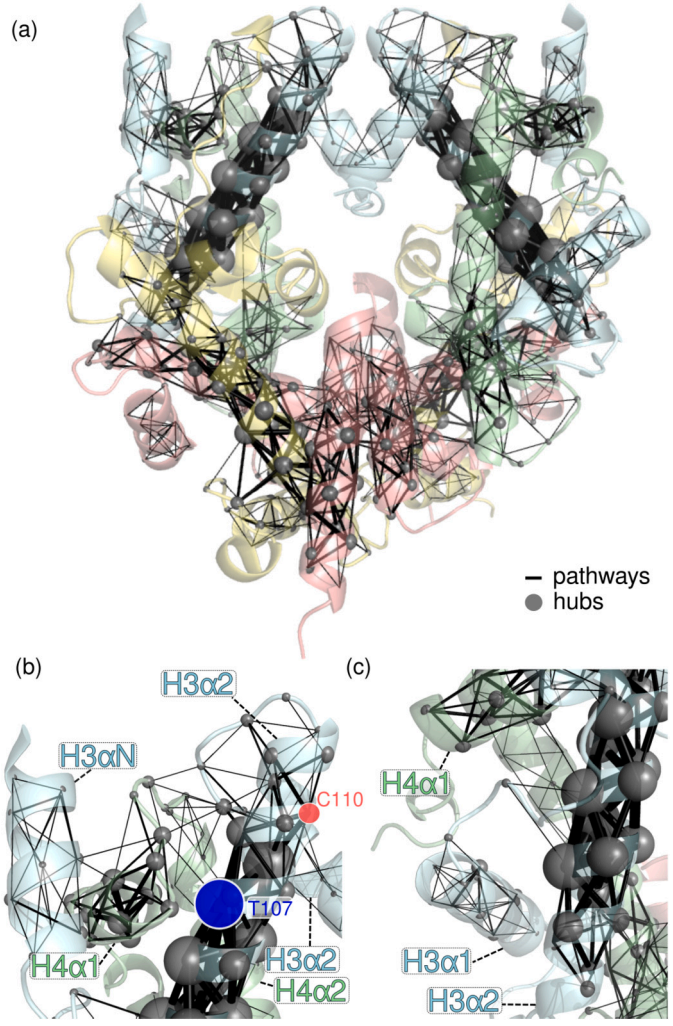

Fig. 3. (a) Mapping of communication pathways (black lines) and hubs (black spheres) in the α-satellite NCP. The larger the line/sphere, the more populated the pathway/hub. **(b)** Pathways around the top of the H3 α2 helix, connecting H3 αN and α2 to H4 α1. C110 and T107 are displayed as red and blue circles, respectively. **(c)** Pathways at the bottom of the H3 α2 helix, showing few connections with the L1 loop after H3 α1.

mostly responsible for communication blocks 5 and 13 identified previously. Less populated hubs are also observed in H2B α2, mostly from A55 to V66. Overall, H2A-H2B hubs appear much less dense than hubs in the H3-H4 dimers, which also explains why communication blocks in H2A-H2B are more fragmented.

Pathways analysis in the 601 NCP resulted in the same trends as for the α-satellite system. The only difference one can observe is a higher density of communication pathways between the histone helices, which translates into the more compact communication blocks as observed above - see Figure S1. However, the density of the communication hubs remains the same, with the H3 α2 helix exhibiting the highest contribution to the overall pathways.

3.2. S-sulfonylation reshapes the H3-H3 contacts by rewiring the local interaction network

3.2.1. Local perturbation of the H3-H3 contacts

In the NCP structure, the bundle formed by H3 and H3' α2 and α3 helices is of crucial importance for the $(H3\text{-}H4)_2$ tetramer assembly. H3C110 hyperoxidation into its sulfonylated counterpart (OCS) induces a rewiring of the local interaction network at the H3-H3 interface, perturbing the stable canonical architecture.

The most pronounced structural change is induced by the rotation of H3'R129 side chain to form a hydrogen bond with OCS, which provokes the displacement of H3 and H3' α2 helices ends - see Fig. 4. The representative structures and corresponding distance values are showed only for the first MD replicate, but this phenomena is observed in all the MD replicates - see Figure S3. At the beginning of the simulation, the structure of the NCP bearing OCS is very close to the unmodified one (in purple and transparent blue, respectively in Fig. 4-a). However, a conformational change is observed after ~100 ns of simulation, with the rotation of R129' inwards to interact with OCS, that pushes H3 and H3' α2 helices away from each other for the rest of the simulation - see Fig. 4-b. Interestingly, the α3 helix position is very weakly perturbed by these changes, as suggested by a very modest drift of the CA backbone atom position of R129' (1.7 ± 0.4 Å for MD1, 1.8 ± 0.6 Å over all MD replicates) compared to its CZ side chain atom (5.6 ± 1.0 Å for MD1, 5.0 ± 1.5 Å over all MD replicates), as showed in Fig. 4-c. On the contrary, a pronounced drift of OCS CA atom with respect to its initial position is observed (3.2 ± 0.7 Å for MD1, 2.7 ± 1.1 Å over all MD replicates), which illustrates the displacement of H3 α2 helix end. The evolution of the distances between the center of mass of the H3 and H3' α2 helices ends (taken as residues 105-115 and 105'-115') also shows that these helices are moving away from each others, with an overall increase of ~ 3.5 Å and an average distance of 16.1 ± 0.8 Å compared to a value of 12.5 ± 0.2 Å in the control simulations - Fig. 4-d. Interestingly, while H3'R129 is initially close enough to H3E105 to form a salt bridge, this interaction does not hold upon the presence of OCS, with which R129' interacts preferentially as illustrated by the increase of the distance between R129' CZ and E105 CD atoms (from ~ 7 Å to ~ 13 Å, average of 12.4 ± 1.4 Å) and the decrease of the distance between R129' NH2 and OCS SG atoms (from ~ 13 Å to ~ 4 Å, average of 4.6 ± 2.0 Å).

The displacement of H3 and H3' helices also involves some changes in the canonical interaction patterns of the four-helix bundle. One very stable symmetrical hydrogen bond in the non-modified NCP simulations is found between H113 and D123 on the facing H3 copy, with an average distance between H113 HE2 and D123 CG atoms of 3.3 ± 0.3 Å for both NCP sides - see Figures S4 and S5. In the simulations with OCS these interactions are destabilized, especially for the one with H113 on the same H3 copy as OCS (i.e., H113-D123'). Average distances are in this case increased to 10.7 ± 3.2 Å (H113-D123') and 4.3 ± 1.2 Å (H113'-D123). The presence of OCS might induce steric and electrostatic hindrance that prevents the formation of the canonical hydrogen bond network. The mapping of the hydrogen bond networks perturbation confirms the aforementioned loss and gain of interactions, and also revealing longer-range impact on the interaction between histones H3 C-termini and the H2A-H2B dimers - see Figure S6. Of note, same results are found for simulations with 0M NaCl - see Figure S7.

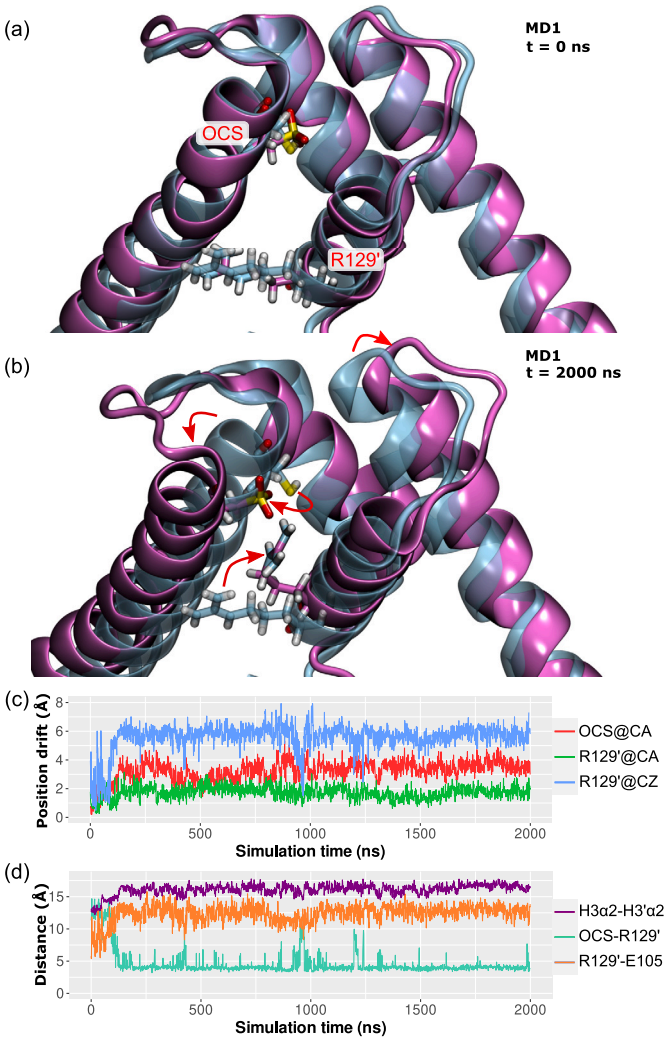

Fig. 4. Superposition of the S-sulfonylated structure (purple) at **(a)** t = 0 ns and **(b)** at t = 2000 ns of the MD1 replicate onto the unmodified crystal structure (transparent cyan). Both copies of histone H3 are shown. The OCS sulfonylated residue and R129' on the facing copy are displayed in licorice to illustrate their interaction upon sulfonylation. **(c)** Positional drift (in Å) of OCS CA atom (red) and R129' CA (green) and CZ (blue) atoms along the MD1 replicate. It is calculated along the simulation as the distance of each atom to its initial position in the crystal structure. **(d)** Evolution of the distances between the ends of the histones H3 α2 helices (taken as the residues 105 to 115, in purple), between OCS SG atom and R129' NH2 atom (cyan), and between R129' CZ atom and H3E105 CD atom (orange).

Simulations with an additional S-sulfonylated site on H3'C110 show similar trends, with denser blocks in the H2A-H2B dimers compared to the canonical system - see Figure S7. However, the second modification site induces larger structural deviations at the H3-H3' contact surface, with stronger deformations of the H3α3 helix that can locally unfold due to the rewiring of the local interaction network - see Figure S8. Indeed, it induces the apparition of an additional negative charge in the H3-H3' bundle, which attracts the surrounding positively charged residues located mainly on the H3 and H3' α3 helices. As in the system with a single modification, OCS110 interacts with both R129' and H113' - see Figure S9. The second S-sulfonylated site, OCS110', interacts with R129 and H113, but eventually also with R131 and K122, resulting in potentially strong deformations of the H3 α3 helix.

3.2.2. Rewiring of the communication blocks and pathways

The perturbation of the local interactions network near OCS results in a re-shaping of the overall communication blocks - see Fig. 5-a. Noteworthy, the H2A-H2B dimers exhibit bigger blocks than in the unmodified system. On face A, three blocks can be distinguished that independently gather H2A α3 and H2B α1-2 (Block 1), H2B α3 (Block 2), and H2A α1-2 and H2B αN (Block 3). On face B, only two blocks are found, with the H2B α3 still isolated in Block 5 and the rest of the H2A-H2B α helices all gathered in Block 6. Besides, H3-H4 dimers are deferentially impacted, rather it is on OCS side or not. On face A, a single block is observed (Block 4), whereas on face B H3 α3 does not communicate with the other helices and H3 α1 is isolated in Block 8. The other helices are gathered in the large Block 9. Interestingly enough, the OCS residue is located in Block 9, while the H3 α3 helix that faces it is disconnected from the rest of the dimer, with only a small communication block (Block 7) of four amino acids (Q125, A127, R129, R131).

A closer look into the communication pathways allows to gain insights into the molecular mechanisms behind the blocks reorganization. The overall map of the pathways reveals an increase of the hubs importance in H3 and even H2A α2 helices - see Fig. 5-b. The same H2A α2 hubs are found compared to the canonical NCP, but they funnel an increased number of inter-helices pathways within H2A-H2B, explaining the presence of larger communication blocks in these dimers. Of note, both H2A-H2B dimers show enhanced communication pathways, yet this trend is even more pronounced for face B than face A, which also rationalize the asymmetry of the blocks - see Figure S2.

The major hubs in H3 α2, already observed in the unmodified NCP, are also found to be more populated upon S-sulfonylation. At the bottom of this helix, the communication network between H3 α1, and H4 α1-3 shows much more connections - see Fig. 5-c. At its top, an asymmetry between H3 (bearing OCS) and H3' is observed, as one could expect. On H3', communication pathways are found similar to the canonical NCP, yet the hubs importance appear to be slightly increased. On H3, where OCS perturbs the interaction network as above-described, there is a drastic loss of connection between H3 α2 and α3 helices, which decreases the importance of the neighboring hubs such as T107 - 5-d. Weak pathways are found in H3 α3 but they remain isolated, with no connection to the other helices. The hydrogen bond network analysis shows a reorganization of the interactions around the OCS residue, and a loss of contacts between the H3/H3' C-termini and H2A and H4 - see Figure S6.

Interestingly, while salt concentration does not have any effect on the communication pathways, the addition of a second modification site on H3' only results in the loss of communication pathways in H3'α2. This effect remains very local, and does not spread onto the entire NCP architecture, suggesting that a single S-sulfonylated site is already enough to induce a maximal structural signature - see Figure S10.

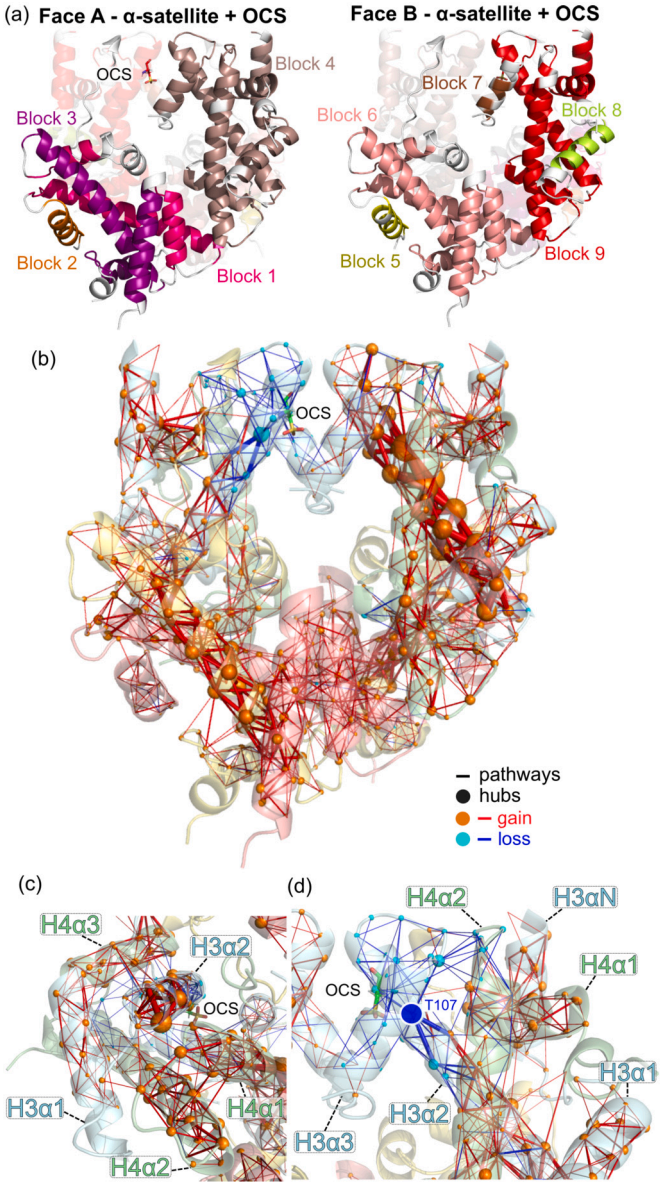

Fig. 5. (a) Communications blocks in the α-satellite NCP with cysteine S-sulfonylation (OCS), on face A and face B. **(b)** Perturbation of communication pathways upon S-sulfonylation, viewed from face B. Red paths/hubs are gains with the modification, blue are losses. **(c)** Bottom view of H3' α2 helix (in communication Block 4), through which multiple pathways connect other H3' and H4' helices. **(d)** Weakened pathways around the S-sulfonylated cysteine. T107 is highlighted by a white-blue circle.

3.3. S-sulfonylation destabilizes DNA near the dyad

3.3.1. Increased DNA flexibility at SHL0/SHL-1

Besides the extensive description of histone core communication networks and their rewiring by S-sulfonylation, the impact of this modification on the DNA helix structure and dynamics was also assessed. The structural descriptor that was the most impacted by histone H3 S-sulfonylation is the flexibility of the nucleic acids in the dyad region. The per residue contribution to the overall DNA flexibility was computed for the S-sulfonylated system and the unmodified one. The mapping of the deviation of these contributions upon S-sulfonylation reveals an increase of flexibility not only at the DNA entry/exit sites but also, more interestingly, near the dyad (SHL0) - see Fig. 6-a. In the nucleosome structure, the dyad region is the most stable part of nucleosomal DNA, and DNA-protein interactions near this axis have a crucial role for nucleosome stability and the regulation of its assembly/disassembly [14,18,17]. The hyperoxidation of histone H3 C110 results in an asymmetric destabilization of the dyad region, with a more pronounced effect on the SHL0/SHL-1 region opposite to the PTM site (i.e., not directly above the PTM). The DNA entry/exit are also destabilized by the presence of OCS, with a much more pronounced effect on the side of the NCP opposite to OCS - Face B, see 6-b. However, this only concerns less than 10 base-pairs (bp) sections on DNA termini. Noteworthy, weak deviations are also observed on longer-range distances: a very localized stiffening of nucleotides (dA174 and dA175 at SHL-4.5, dC237 and dT238 at SHL1.5), and a slight destabilization of strand1 at SHL4/4.5.

Simulations with two OCS sites show similar results characterized by a destabilization of the dyad - see Figure S11. Of note, few deviations can be pinpointed that might result from differential interactions with H2A and H4' N-term tails: a lower flexibility in the SHL3.5 region (residues 45-47 and 250-252), and a higher flexibility on the solvent-exposed strand at SHL4.5 (residues 265 and 266).

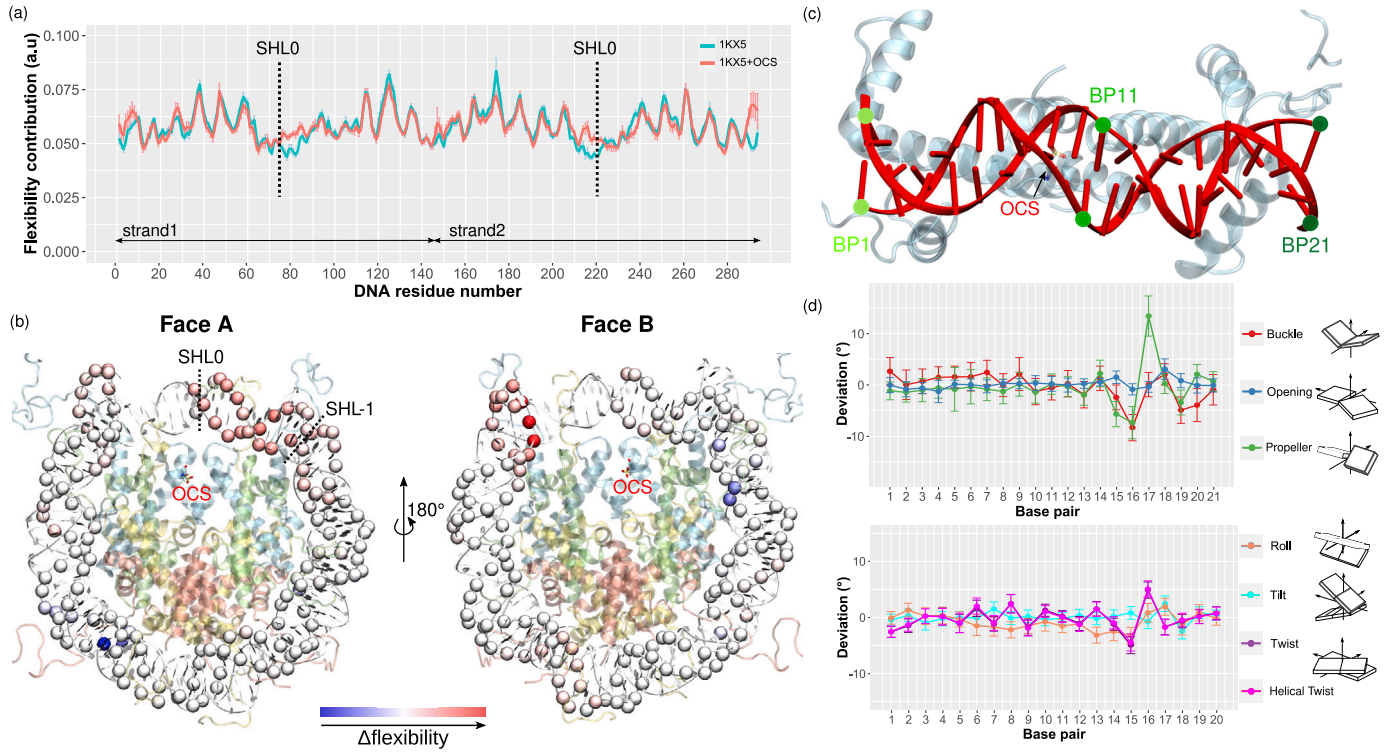

Fig. 6. (a) Per residue flexibility contribution of the two DNA strands. SHL0 is indicated as it is, besides the DNA entry/exit, the region the most perturbed by OCS. **(b)** Projection of the perturbation of the per residue flexibility in DNA upon S-sulfonylation, with respect to the unmodified system. Red: higher flexibility, blue: lower flexibility, white: no perturbation. The S-sulfonylated cysteine is displayed in licorice and superhelical locations SHL0 and SHL-1 are indicated on Face A to highlight the enhanced flexibility in this region. **(c)** Top view of the 21-bp DNA section taken for the structural parameters calculation (i.e., between SHL+1 and SHL-1). Base pairs 1, 11, and 21 are labeled in green. Histones H3 and OCS are displayed in transparent. The remaining of the system is not shown. **(d)** Deviation of the intra- (top) and inter- (bottom) base pair angular parameters of the 21-bp DNA at the dyad in the S-sulfonylated NCP with respect to the unmodified system. Schematic representations of the parameters are provided, with each nucleobase displayed as a square. Inter-base pair parameters are calculated by couples of adjacent base pairs (e.g., bp1-bp2, bp2-bp3).

The destabilization of the dyad is also observed in simulations with one S-sulfonylated site but without NaCl. Mild deviations in the DNA flexibility profile are found compared to the 0.15M NaCl counterpart. This was expected as it is known that salt concentration can influence the stability of the nucleosome [41]. Mostly, some DNA regions are found to be more flexible than in the system with 0.15M NaCl. It is especially the case at SHL1.75 and SHL5. Again, interactions with the nearby histone tails might play a role. In the SHL1.75 region, the H4 tail interacts less in the simulations with 0.15M NaCl but not in the ones without NaCl. This might be the result of a lack of conformational sampling of the histone tails, but overcoming this would require the use of much more costly enhanced sampling methods which remains beyond the scope of the present study.

In order to probe the molecular mechanisms driving the OCS-induced DNA destabilization near the dyad axis, an in-depth structural analysis of the 21-bp section around the dyad axis was performed, and DNA-protein interactions were monitored.

3.3.2. *DNA structural parameters at the dyad*

Structural descriptors of the 21-bp DNA section around the dyad were computed on the MD ensembles with and without S-sulfonylation - see Fig. 6-c and Figures S12 and S13. The OCS-induced deviation of intra-base pair, inter-base pair, and base pair axis parameters did not show any drastic deformation of the DNA double helix, but interestingly the largest perturbations are localized in the second half of the 21-bp section, i.e., in the SHL0/SHL-1 region that was found to experience an enhanced flexibility. For instance, the buckle and propeller angles deviations is more pronounced for base pairs 16 (residues dT217 and d) and 17 (residues dG218 and dC77), corresponding to residues 78-82 and 213-217 on strands 1 and 2, respectively - see Fig. 6-d. This might result from the perturbation of the hydrogen bond network as described in the section below. Likewise, the inter-base pair twist angles exhibit peaks in this region. Noteworthy, helical twist and helical rise (calculated with respect to the overall helical axis) are similar to the base pair twist and rise values (calculated with respect to a single base pair step), respectively, which is characteristic of B-like helices [23].

Overall, S-sulfonylation seems to only weakly perturb the DNA structure at the dyad, yet the largest deviations of the structural parameters with respect to the unmodified system are found in the SH0/SHL-1 region for which the flexibility was increased with the presence of OCS. Of note, these trends are conserved in simulations with two modification sites (see Figures S14 and S15), and the salt concentration also does not change these observations - see Figures S16 and S17.

3.3.3. *Interactions between DNA and the histone core lateral surface*

Canonical interactions between DNA and the histone residues at the lateral surface of the octamer were listed from analysis of the α-satellite NCP experimental structure and from the literature, and monitored in the simulations of the unmodified and S-sulfonylated α-satellite NCP - see Table S2 and Figures S18 and S19. While most of the hydrogen bonds and salt bridges were unchanged by the hyperoxidation of histone H3, some of them located near the dyad exhibited larger deviations in the S-sulfonylated system. It is the case for interactions involving H3'K115 and H3'T118, showing a broader distribution with OCS than in the unmodified system. On histone H3/H3', H3'K115 NZ atom distance to dA220 phosphate is of 7.0 ± 2.0 Å with OCS and 6.1 ± 1.1 Å without, and K115' NZ atom distance to dA73 phosphate is of 7.2 ± 1.8 Å with OCS and 6.1 ± 1.2 Å without. Interestingly, the standard deviations of the distance between H3'T118 HG1 and dG218 phosphate is larger with OCS (3.2 ± 0.9 Å with OCS vs 2.9 ± 0.2 Å without),

which results from the hydrogen bond network rewiring induced by the H3 helices displacement aforementioned. Indeed, the mapping of the hydrogen bond network showed an enhanced interaction between H3'T118 and H4'R45, which might weaken their contact with other partners including DNA - see Figure S6. This reorganization participates to the increase of the DNA flexibility in contact with H3'T118 and H4'R45 (SHL0/SHL-1), and even allows for very local sliding events where H3'T118 interaction with dG218 shifts to dT217 - see Figure S20 and supplementary video. Indeed, we observed in one of the replicates such a stable shift, and in the other replicates some peaks are found in the monitoring of the H3'T118@SG - dG218@P distance. This suggests that the sulfonylation of H3C110 can impact this DNA-histone contact site, located 20 Å away, and destabilize very locally the positioning of the double helix on the histone core through an allosteric process. Importantly, histones H2A C-term and H3 N-term tails can also interact in this region of the DNA, which might also influence the base-pair parameters. This local sliding event is also observed in the simulations with two modification sites, yet only at the end of one of the replicates. This phenomenon might constitute a rare event, hard to access in the time-scales we can sample with unbiased MD simulations. Future investigations using enhanced sampling would allow to better probe the relevance of this phenomenon upon histone PTM.

Of note, the flexibility analysis of the protein dimers did not show any drastic deviation upon S-sulfonylation in the structured parts of the histone core, yet the H3 α3 helix facing the OCS site exhibits a mild increase which is not observed in its H3' non-modified counterpart - see Figure S21. This is only slightly different upon the addition of a second sulfonylated site (localized on H3' α3), and is not influenced by the salt concentration - see Figure S22.

4. Discussion

Owing to extensive all-atom molecular dynamics simulations and in-depth structural analysis, we described the communication networks within the histone core of the canonical NCP with both α-satellite and 601 Widom sequence. We also investigated their perturbation upon hyperoxidation of histone H3C110, showing that the S-sulfonylation PTM of this residue results in the destabilization of the DNA at the dyad and a rewiring of the interactions network within the histone core.

The detailed map of the communication pathways within the canonical NCP offers a novel way to apprehend how histone proteins synergetically interact with one another. Our results show that communication blocks are localized in separate H2A-H2B or H3-H4 units, i.e., no inter-dimer communication pathways are observed - see Figs. 2 and S1. This 'per dimer' organization is in good agreement with the fact that the H2A-H2B dimer is more fragmented, which underlines a less compact interaction network than in their H3-H4 counterparts. In this sense, it is interesting to underline that the plasticity of H2A–H2B is required for nucleosome stability [42]. Despite their more intense intrinsic communication networks H3-H4 dimers do not share any communication pathway, which could explain why experiments showed that H3-H4 dimers are found to be very stable while the $(H3\text{-}H4)_2$ tetramer remains less stable than the H2A-H2B dimer [43]. Interestingly, while only very weak differences are observed with the 601 Widom sequence compared to the α-satellite NCP, larger communication blocks are found within the dimers, suggesting a more compact architecture which might result from the tighter packing of DNA (146-bp vs 147-bp in the α-satellite sequence) - see Fig. 2-a and S1.

The in-depth analysis of communication pathways allowed to pinpoint key-residues acting as communication hubs within the NCP structure, for both 601 and α-satellite sequences. The most connected hubs are found in histone H3 α2 helix (M90 to T107), which funnel extensive communication pathways within the H3-H4 dimer - see Fig. 3. None of them undergo PTM, except T107 that can be phosphorylated [44]. Noteworthy, C110 is directly connected to T107, suggesting that its modification might have important consequences on the H3-H4 communication network as we observed for S-sulfonylation. Likewise, only few residues in H4 α1 and H2A α2 largest hubs are known to be PTM sites (H4K31 and H2AT59). As was already observed for point mutations [40], PTM sites are important to regulate the system's structure, but they are not necessarily large communication hubs and instead are most frequently located in their vicinity. Interestingly enough, few of these hubs are also mutational hotspots in several types of cancer (H3E97, H3E105, H2AE56) [45].

Noteworthy, the communication pathways are exclusively found in the structured histone core, not on the tails. As PTM on the histone tails are mostly involved in partner protein-mediated regulation of the nucleosome architecture or direct modulation of DNA-tails interactions, PTM in the histone core might have a different role with a direct influence onto DNA-histone interactions and nucleosome dynamics [46]. Besides, we identified the most populated hubs on the H3 and H2A, which are known to be the two histone types with the most variants. This further underlines their crucial role in the regulation of the nucleosome dynamical behavior. However, it is important to underline that the COMMA2 analysis of the communication networks does not include the DNA helix, yet communication pathways might also transit through it via histone-DNA interactions as previously suggested by Bowerman and Wereszczynski [19]. These results nevertheless provide an in-depth description of the histone units cooperativity, and the next step will be to improve COMMA2 towards the inclusion of DNA in the network analysis.

Histone H3 are the only units bearing cysteine residues, a single one at position 110 in the variant H3.2, and two at positions 96 and 110 in variants H3.1 and H3.3. C110 is located in the four-helix bundle at the H3-H3 interface and is known to undergo diverse types of oxidative PTM [7]. Our simulations brought insights into the structural impact of S-sulfonylation, a PTM resulting from cysteine hyperoxidation, which revealed that this modification impacts not only the histone core intrinsic communication pathways, but also destabilizes the DNA structure near the dyad axis. Generally, PTM located on the lateral surface of the histone core and in contact with the dyad DNA (H4S47ph, H3K115ac, H3T118ph, H3K122ac) are supposed to promote the nucleosome disassembly by directly impairing histone-DNA interactions [18,16]. In the case of H3C110 S-sulfonylation, the structural effect is not direct, because C110 side chain is located ~15 Å away from any nucleic acid. Instead, this modification induces a reorganization of the interaction network, stabilizing the four-helix bundle at the H3-H3 interface, resulting in the displacement of the H3 α2 helices - see Fig. 4. This rearrangement is induced by the rotation of the H3R129' side chain, that comes to interact with the modification site (OCS) and pushes the H3α2 helices away from each other. This also results in the disruption of the very stable H113-D123' and H113'-D123 interactions that maintain the four-helix bundle in the canonical NCP. Long-range effects are observed, with a weakening of the H3-H4 communication pathways and hubs within a radius of ~20 Å from the OCS site, and the perturbation of the hydrogen bonds network especially near H3/H3' C-termini through the disruption of interactions with H2A and H4 - see Figure S6. Such a reorganization of the interaction patterns within the histone core even perturbs the histone-DNA contact, with some very local sliding events observed at SHL0.5 that result from the perturbation of the interactions between H3'T118 and dG218 - see Figure S20 and supplementary video. However, upon OCS the global communication pathways are more intense and hubs get denser in both H3' α2 and H2A α2, with larger communication blocks over the NCP structure. These observations suggest that the S-sulfonylation might destabilize the H3-H3 interface and nearby specific DNA-histone contacts while on the other hand stabilizing each separate dimer, which could be important for promoting the nucleosome disassembly process. Noteworthy, this is in line with the fact that the H2A-H2B plasticity is required for the nucleosome stability, and that some chromatin remodelers require distortions of the histone core for DNA sliding and octamer eviction [47].

Besides the histone core architecture, H3C110 S-sulfonylation also destabilizes DNA near the dyad axis. The latter is normally the most strongly positioned part of the DNA in the nucleosome, and is the last region of DNA to be detached from the $(H3\text{-}H4)_2$ tetramer during the nucleosome disassembly [48]. We showed here that the DNA section between SHL0 and SHL-1 exhibits an increased flexibility upon histone H3 S-sulfonylation, not directly above the modification site but symmetrically to the dyad axis - see Fig. 6-a and b. This effect seems to result from very fine structural effects linked to the OCS-induced H3 $\alpha 2$ helices displacement. While the DNA-protein contacts at the histone core lateral surface exhibit the same patterns in the canonical and hyperoxidized NCP structures, the distribution of hydrogen bonds involving H3T118' (SHL-1) and H3K115 (SHL0) are broader upon OCS, suggesting less stable interactions in these regions. Likewise, the base pairs structural parameters within the SHL+1/SHL-1 DNA section exhibit only weak deviations, yet they are mostly located in the SHL0/SHL-1 region which is also the one exhibiting an enhanced flexibility - see Fig. 6-c and d. These observations suggest that S-sulfonylation destabilizes DNA at the dyad in an indirect way, through a subtle reorganization of the interaction network in the H3-H4 dimers.

The addition of a second modification does not perturb the system strongly more. Indeed, the DNA flexibility and the communication blocks mostly remain the same, while the communication pathways are only locally weakened in the H3 helix bearing the second modification site. A single S-sulfonylated cysteine might be enough to induce a maximal structural signature in the nucleosome core particle, which might be important to trigger a response from remodeling complexes binding or other events leading to nucleosome disassembly. Nevertheless, this remains hypothetical and should be verified by experimental means.

Noteworthy, the dyad destabilization is not influenced by the salt concentration as showed by our simulations with and without the NaCl salt. However, while the DNA flexibility profile is rather similar to the simulations at 0.15M NaCl, some locations are found to be significantly more flexible, which might be due to different interactions with the histone tails. Noteworthy, a computational work based on coarse grain models showed that salt concentration can indeed impact the histone tail conformations [49]. Future investigations with enhanced sampling methods would provide important insights into such effects.

Of course, histone PTM rarely happen alone and oxidative stress conditions might result in the modification of other residues besides H3C110, which could have a synergistic effect on the nucleosome dynamics. Interestingly, several experimental studies about C110 modifications and mutants impact onto the H3-H4 tetramer and overall NCP structure have shown that such chemical change can induce chromatin opening (i.e. by S-glutathionylation) [13], can promote left-to-right-handedness of DNA wrapping on tetrasomes [50,51], can destabilize the $(H3\text{-}H4)_2$ tetramer stability [52], and can influence the nucleosome assembly [53]. More experimental investigations are needed to confirm the role of S-sulfonylation and its interplay with other PTM in the nucleosome disassembly process upon oxidative stress.

Noteworthy, experimental data about histone H3 S-sulfonylation formation and function are scarce, and it is not known if this modification occurs before or after the assembly of the nucleosome. H3C110 is highly buried within the nucleosome structure, but it is known that S-glutathionylation (a much more bulky PTM) can be formed in the nucleosome context. Hence, it is reasonable to hypothesize that cysteine reaction with reactive oxygen species (ROS) could allow the formation of S-sulfonylated C110 in the nucleosome, which might play a different role than in free histones (e.g., nucleosome destabilization vs hindering of histone chaperone binding). Again, experimental investigations could shed light on this point.

5. Conclusion

Among the variety of epigenetic marks regulating DNA compaction, oxidative PTM are very little studied. Resorting to extensive molecular dynamics simulations and in-depth structural analysis, we described the intrinsic communication networks within the canonical NCP and how they are re-shaped by S-sulfonylation of histone H3. This PTM results from the hyperoxidation of H3C110 upon oxidative stress conditions. We showed it induces subtle structural rearrangements that not only impact the histone core plasticity, but also destabilize histone-DNA interactions near the dyad axis allowing very local DNA sliding events. Our results suggest that a single S-sulfonylated cysteine is enough to provoke a specific structural signature in the nucleosome core particle, and that the introduction of a second modification only induce mild, local additional perturbations. These investigations constitute the first extensive insights into the alteration of the NCP communication pathways by a histone oxidative modification. Our results suggest that upon oxidative stress S-sulfonylation might contribute to the standard mechanisms promoting nucleosomal disassembly, and they provide an atomic-scale description of the mechanistic details underlying this process. This work provides an important computational framework for the study of other PTM, disease-related mutations, and histone variants effects onto the nucleosome architecture, that will shed light onto the finely-tuned mechanisms underlying DNA compaction regulation.

Declaration of competing interest

The authors declare that they have no known competing financial interests or personal relationships that could have appeared to influence the work reported in this paper.

Acknowledgement

This work was granted access to the HPC resources IDRIS under the allocation 2022-A0120713412 made by GENCI. E.B. thanks the Explor computing center for computational resources (Grant 2019CPMXX0983), and the Centre National de la Recherche Sciencitifique for her welcome package. E.B. is grateful to Dr. Tao Jiang and Prof. Elise Dumont for providing flexibility analysis scripts.

Appendix A. Supplementary material

All inputs files and representative pdb structures of the systems obtained from extensive molecular dynamics simulations are provided on Github:
https://github.com/emmanuellebignon/NCP-OCS-pathways.

Supplementary material related to this article can be found online at https://doi.org/10.1016/j.csbj.2024.03.025.

References

[1] Davey CA, Sargent DF, Luger K, Maeder AW, Richmond TJ. Solvent mediated interactions in the structure of the nucleosome core particle at 1.9 Å resolution. J Mol Biol 2002;319(5):1097–113. https://doi.org/10.1016/S0022-2836(02)00386-8.
[2] Luger K, Mäder AW, Richmond RK, Sargent DF, Richmond TJ. Crystal structure of the nucleosome core particle at 2.8 Å resolution. Nature 1997;389(6648):251–60. https://doi.org/10.1038/38444.
[3] Garcia-Saez I, Menoni H, Boopathi R, Shukla MS, Soueidan L, Noirclerc-Savoye M, et al. Structure of an H1-bound 6-nucleosome array reveals an untwisted two-start chromatin fiber conformation. Mol Cell 2018;72(5):902–15. https://doi.org/10.1016/j.molcel.2018.09.027.
[4] Henikoff S. Nucleosome destabilization in the epigenetic regulation of gene expression. Nat Rev Genet 2008;9(1):15–26. https://doi.org/10.1038/nrg2206.
[5] Armeev GA, Gribkova AK, Pospelova I, Komarova GA, Shaytan AK. Linking chromatin composition and structural dynamics at the nucleosome level. Curr Opin Struct Biol 2019;56:46–55. https://doi.org/10.1016/j.sbi.2018.11.006.
[6] Bignon E, Allega MF, Lucchetta M, Tiberti M, Papaleo E. Computational structural biology of S-nitrosylation of cancer targets. Front Oncol 2018;8:272. https://doi.org/10.3389/fonc.2018.00272.
[7] García-Giménez J-L, Garcés C, Romá-Mateo C, Pallardó FV. Oxidative stress-mediated alterations in histone post-translational modifications. Free Radic Biol Med 2021;170:6–18. https://doi.org/10.1016/j.freeradbiomed.2021.02.027.
[8] García-Giménez JL, Romá-Mateo C, Pallardó FV. Oxidative post-translational modifications in histones. BioFactors 2019;45(5):641–50. https://doi.org/10.1002/biof.1532.

[9] Sha Y, Marshall HE. S-nitrosylation in the regulation of gene transcription. Biochim Biophys Acta G, Gen Subj 2012;1820(6):701–11. https://doi.org/10.1016/j.bbagen.2011.05.008.
[10] Marinho HS, Real C, Cyrne L, Soares H, Antunes F. Hydrogen peroxide sensing, signaling and regulation of transcription factors. Redox Biol 2014;2:535–62. https://doi.org/10.1016/j.redox.2014.02.006.
[11] Kim Y-J, Kim D, Illuzzi JL, Delaplane S, Su D, Bernier M, et al. S-glutathionylation of cysteine 99 in the APE1 protein impairs abasic endonuclease activity. J Mol Biol 2011;414(3):313–26. https://doi.org/10.1016/j.jmb.2011.10.023.
[12] Tang C-H, Wei W, Liu L. Regulation of dna repair by S-nitrosylation. Biochim Biophys Acta G, Gen Subj 2012;1820(6):730–5. https://doi.org/10.1016/j.bbagen.2011.04.014.
[13] García-Giménez JL, Olaso G, Hake SB, Bönisch C, Wiedemann SM, Markovic J, et al. Histone H3 glutathionylation in proliferating mammalian cells destabilizes nucleosomal structure. Antioxid Redox Signal 2013;19(12):1305–20. https://doi.org/10.1089/ars.2012.5021.
[14] Simon M, North JA, Shimko JC, Forties RA, Ferdinand MB, Manohar M, et al. Histone fold modifications control nucleosome unwrapping and disassembly. Proc Natl Acad Sci 2011;108(31):12711–6. https://doi.org/10.1073/pnas.1106264108.
[15] Bowman GD, Poirier MG. Post-translational modifications of histones that influence nucleosome dynamics. Chem Rev 2014;115(6):2274–95. https://doi.org/10.1021/cr500350x.
[16] Chatterjee N, North JA, Dechassa ML, Manohar M, Prasad R, Luger K, et al. Histone acetylation near the nucleosome dyad axis enhances nucleosome disassembly by RSC and SWI/SNF. Mol Cell Biol 2015;35(23):4083–92. https://doi.org/10.1128/MCB.00441-15.
[17] North JA, Šimon M, Ferdinand MB, Shoffner MA, Picking JW, Howard CJ, et al. Histone H3 phosphorylation near the nucleosome dyad alters chromatin structure. Nucleic Acids Res 2014;42(8):4922–33. https://doi.org/10.1093/nar/gku150.
[18] Tropberger P, Pott S, Keller C, Kamieniarz-Gdula K, Caron M, Richter F, et al. Regulation of transcription through acetylation of H3K122 on the lateral surface of the histone octamer. Cell 2013;152(4):859–72. https://doi.org/10.1016/j.cell.2013.01.032.
[19] Bowerman S, Wereszczynski J. Effects of macroH2A and H2A.Z on nucleosome dynamics as elucidated by molecular dynamics simulations. Biophys J 2016;110(2):327–37. https://doi.org/10.1016/j.bpj.2015.12.015.
[20] Phillips JC, Hardy DJ, Maia JD, Stone JE, Ribeiro JV, Bernardi RC, et al. Scalable molecular dynamics on cpu and gpu architectures with namd. J Chem Phys 2020;153(4):044130. https://doi.org/10.1063/5.0014475.
[21] Case D, Belfon K, Ben-Shalom I, Brozell S, Cerutti D, Cheatham III T, et al. Amber 2020. San Francisco: University of California; 2020.
[22] Karami Y, Bitard-Feildel T, Laine E, Carbone A. "Infostery" analysis of short molecular dynamics simulations identifies highly sensitive residues and predicts deleterious mutations. Sci Rep 2018;8(1):16126. https://doi.org/10.1038/s41598-018-34508-2.
[23] Lavery R, Moakher M, Maddocks JH, Petkeviciute D, Zakrzewska K. Conformational analysis of nucleic acids revisited: curves+. Nucleic Acids Res 2009;37(17):5917–29. https://doi.org/10.1093/nar/gkp608.
[24] Humphrey W, Dalke A, Schulten K. VMD: visual molecular dynamics. J Mol Graph 1996;14(1):33–8. https://doi.org/10.1016/0263-7855(96)00018-5.
[25] Schrödinger LLC. The PyMOL molecular graphics system, version 1.8; November 2015.
[26] Maier JA, Martinez C, Kasavajhala K, Wickstrom L, Hauser KE, Simmerling C. ff14SB: improving the accuracy of protein side chain and backbone parameters from ff99SB. J Chem Theory Comput 2015;11(8):3696–713. https://doi.org/10.1021/acs.jctc.5b00255.
[27] Ivani I, Dans PD, Noy A, Perez A, Faustino I, Hospital A, et al. Parmbsc1: a refined force field for DNA simulations. Nat Methods 2016;38(13):55–8. https://doi.org/10.1038/nmeth.3658.
[28] Yoo J, Aksimentiev A. New tricks for old dogs: improving the accuracy of biomolecular force fields by pair-specific corrections to non-bonded interactions. Phys Chem Chem Phys 2018;20(13):8432–49. https://doi.org/10.1039/C7CP08185E.
[29] Bhatt MR, Zondlo NJ. Synthesis and conformational preferences of peptides and proteins with cysteine sulfonic acid. Org Biomol Chem 2023;21(13):2779–800. https://doi.org/10.1039/d3ob00179b.
[30] Hopkins CW, Le Grand S, Walker RC, Roitberg AE. Long-time-step molecular dynamics through hydrogen mass repartitioning. J Chem Theory Comput 2015;11(4):1864–74. https://doi.org/10.1021/ct5010406.
[31] Miyamoto S, Kollman PA. Settle: an analytical version of the SHAKE and RATTLE algorithm for rigid water models. J Comput Chem 1992;13(8):952–62. https://doi.org/10.1002/jcc.540130805.
[32] Darden T, York D, Pedersen L. Particle mesh Ewald: an n·log (n) method for Ewald sums in large systems. J Chem Phys 1993;98(12):10089–92. https://doi.org/10.1063/1.464397.
[33] Smirnova E, Bignon E, Schultz P, Papai G, Ben-Shem A. Binding to nucleosome poises SIRT6 for histone H3 de-acetylation. eLife 2023;12:RP87989. https://doi.org/10.7554/elife.87989.5.
[34] Karami Y, Laine E, Carbone A. Dissecting protein architecture with communication blocks and communicating segment pairs. BMC Bioinform 2016;17(Suppl 2 (Suppl 2)):13. https://doi.org/10.1186/s12859-015-0855-y.
[35] McDonald IK, Thornton JM. Satisfying hydrogen bonding potential in proteins. J Mol Biol 1994;238(5):777–93. https://doi.org/10.1006/jmbi.1994.1334.
[36] Bignon E, Gillet N, Chan C-H, Jiang T, Monari A, Dumont E. Recognition of a tandem lesion by DNA bacterial formamidopyrimidine glycosylases explored combining molecular dynamics and machine learning. Comput Struct Biotechnol J 2021;19:2861–9. https://doi.org/10.1016/j.csbj.2021.04.055.
[37] Bignon E, Claerbout VE, Jiang T, Morell C, Gillet N, Dumont E. Nucleosomal embedding reshapes the dynamics of abasic sites. Sci Rep 2020;10(1):17314. https://doi.org/10.1038/s41598-020-73997-y.
[38] Bignon E, Gillet N, Jiang T, Morell C, Dumont E. A dynamic view of the interaction of histone tails with clustered abasic sites in a nucleosome core particle. J Phys Chem Lett 2021;12(25):6014–9. https://doi.org/10.1021/acs.jpclett.1c01058.
[39] Cutter AR, Hayes JJ. A brief review of nucleosome structure. FEBS Lett 2015;589(20):2914–22. https://doi.org/10.1016/j.febslet.2015.05.016.
[40] Souza VP, Ikegami CM, Arantes GM, Marana SR. Mutations close to a hub residue affect the distant active site of a GH1 β-glucosidase. PLoS ONE 2018;13(6):e0198696. https://doi.org/10.1371/journal.pone.0198696.
[41] Hazan NP, Tomov TE, Tsukanov R, Liber M, Berger Y, Masoud R, et al. Nucleosome core particle disassembly and assembly kinetics studied using single-molecule fluorescence. Biophys J 2015;109(8):1676–85. https://doi.org/10.1016/j.bpj.2015.07.004.
[42] Bilokapic S, Strauss M, Halic M. Histone octamer rearranges to adapt to dna unwrapping. Nat Struct Mol Biol 2018;25(1):101–8. https://doi.org/10.1038/s41594-017-0005-5.
[43] Banks DD, Gloss LM. Equilibrium folding of the core histones: the H3-H4 tetramer is less stable than the H2A-H2B dimer. Biochemistry 2003;42(22):6827–39. https://doi.org/10.1021/bi026957r.
[44] Xu Y-M, Du J-Y, Lau AT. Posttranslational modifications of human histone H3: an update. Proteomics 2014;14(17–18):2047–60. https://doi.org/10.1002/pmic.201300435.
[45] Nacev BA, Feng L, Bagert JD, Lemiesz AE, Gao J, Soshnev AA, et al. The expanding landscape of 'oncohistone' mutations in human cancers. Nature 2019;567(7749):473–8. https://doi.org/10.1038/s41586-019-1038-1.
[46] Tessarz P, Kouzarides T. Histone core modifications regulating nucleosome structure and dynamics. Nat Rev Mol Cell Biol 2014;15(11):703–8. https://doi.org/10.1038/nrm3890.
[47] Sinha KK, Gross JD, Narlikar GJ. Distortion of histone octamer core promotes nucleosome mobilization by a chromatin remodeler. Science 2017;355(6322):eaaa3761. https://doi.org/10.1126/science.aaa3761.
[48] Gansen A, Valeri A, Hauger F, Felekyan S, Kalinin S, Tóth K, et al. Nucleosome disassembly intermediates characterized by single-molecule FRET. Proc Natl Acad Sci 2009;106(36):15308–13. https://doi.org/10.1073/pnas.0903005106.
[49] Arya G, Schlick T. A tale of tails: how histone tails mediate chromatin compaction in different salt and linker histone environments. J Phys Chem A 2009;113(16):4045–59. https://doi.org/10.1021/jp810375d.
[50] Ordu O, Kremser L, Lusser A, Dekker NH. Modification of the histone tetramer at the H3-H3 interface impacts tetrasome conformations and dynamics. J Chem Phys 2018;148(12). https://doi.org/10.1063/1.5009100.
[51] Peterson S, Danowit R, Wunsch A, Jackson V. NAP1 catalyzes the formation of either positive or negative supercoils on DNA on basis of the dimer- tetramer equilibrium of histones H3/H4. Biochemistry 2007;46(29):8634–46. https://doi.org/10.1021/bi6025215.
[52] Banks DD, Gloss LM. Folding mechanism of the (H3-H4)2 histone tetramer of the core nucleosome. Protein Sci 2004;13(5):1304–16. https://doi.org/10.1110/ps.03535504.
[53] Hamiche A, Richard-Foy H. The switch in the helical handedness of the histone (H3-H4) 2 tetramer within a nucleoprotein particle requires a reorientation of the H3-H3 interface. J Biol Chem 1998;273(15):9261–9. https://doi.org/10.1074/jbc.273.15.9261.